Research Article | Vol. 13, No. 12 / 1 Dec 2023 / Optical Materials Express 3653
Optical Materials EXPRESS

Effects of high-power laser radiation on polymers for 3D printing micro-optics

Sebastian Klein,[1,†] Pavel Ruchka,[1,*,†] Thomas Klumpp,[2] Nils Bartels,[1] Tobias Steinle,[1] and Harald Giessen[1]

[1]4th Physics Institute and Research Center SCoPE, University of Stuttgart, Pfaffenwaldring 57, 70569 Stuttgart, Germany
[2]Deutsches Zentrum für Luft- und Raumfahrt (DLR), Institut für Technische Physik, Pfaffenwaldring 38-40, 70569 Stuttgart, Germany
[†]These authors contributed equally
[*]p.ruchka@pi4.uni-stuttgart.de

Abstract: 3D printing has become a widely used technique for manufacturing micro-optical components for sensing, measurements, biomedical and quantum technologies. Hence, knowing the maximum usable power or damage thresholds of 3D-printed micro-optics becomes crucial. Here we present a first study of the damage threshold values of the IP-S photoresist under high-power cw-, fs-, and ns-pulsed laser radiation with wavelengths in the NIR range. We also study the differences between visual evaluation using bright-field microscopy, DIC-microscopy, and beam-profile damage detection. Finally, we present several application-inspired use cases of 3D printed fiber micro-optics, reaching 10.5 W output power of cw-radiation at 915 nm and 4.5 W and 550 fs pulsed operation at 1040 nm.

1. Introduction

Since 3D-printed micro-optics became a widespread field, many use cases were highlighted within various directions of research [1–3]. While some of the already existing works about 3D-printed optics focus rather on the optical performance in terms of image or beam quality produced by the 3D-printed optics [4–9], others discuss the application-related performance [10–15]. In some studies the authors already discussed the problem of laser damage thresholds when using 3D-printed micro-optics [16,17], although only in particular use cases for a specific optical design. So far, there were no systematic studies on the damage thresholds of photomolymers. This is a crucial aspect, since the ability to withstand high-power laser radiation is not only a limiting factor in some already existing applications such as sensing, biomedical and quantum technologies [18–20], but knowing the thresholds might result in new use cases emerging, for instance, lasers incorporating 3D-printed optics or µm-precise material processing. Previously in [21,22], laser-induced damage threshold (LIDT) tests were performed for different photopolymers at various wavelengths with ns- and fs-pulsed laser radiation. In a recent work [23], the authors use calcination to increase the damage threshold of a photopolymer SZ2080^{TM}. However, in a wide variety of scientific and industry applications, Nanoscribe GmbH photopolymers are used, and hence the need for determination of the corresponding damage threshold values exists.

Here, we conduct a series of experiments using various types of laser radiation to study the damage threshold values of IP-S photopolymer (Nanoscribe GmbH). We study the thresholds for fs-radiation under different wavelengths and exposure times. We also examine the effects of thermal lensing separately from the permanent damage induced by the high-power exposure. In addition, we conduct experiments under high-power ns-pulsed laser radiation according to the ISO 21254 [24] and compare the results to our fs-tests. Finally, we present several application

#503929 https://doi.org/10.1364/OME.503929
Journal © 2023 Received 22 Aug 2023; revised 13 Nov 2023; accepted 19 Nov 2023; published 29 Nov 2023

Optical Materials EXPRESS

examples of 3D-printed micro-optics, which operate at 10.5 W power using cw-radiation at 915 nm and 4.5 W for fs-pulsed radiation at 1040 nm. These examples highlight the possibility to use such 3D-printed optics within applications, where high output power is of critical importance.

2. Methods

For damage testing we use the setup depicted in Figure 1(a). To expose the samples, we use a combination of an SI Stuttgart Instruments GmbH Primus 1040 nm pump-laser, which delivers an output power > 6 W with a pulse duration of < 550 fs and a repetition rate of 40 MHz, with an SI Stuttgart Instruments GmbH Alpha tunable frequency converter. This combination allows us to perform the experiments in a broad wavelength-range from 1350 nm to 2050 nm with the signal output. For wide-range power control we use a half-wave plate in combination with a polarizing beam-splitter, therefore, fast intensity-variations without the need of changing parameters of the frequency converter are possible. To additionally control the duration of high-power exposures we use an electronically controlled mechanical shutter Uniblitz VS25 in combination with an Uniblitz VCM-D1 shutter driver, which allows us to set the exposure time in the millisecond regime.

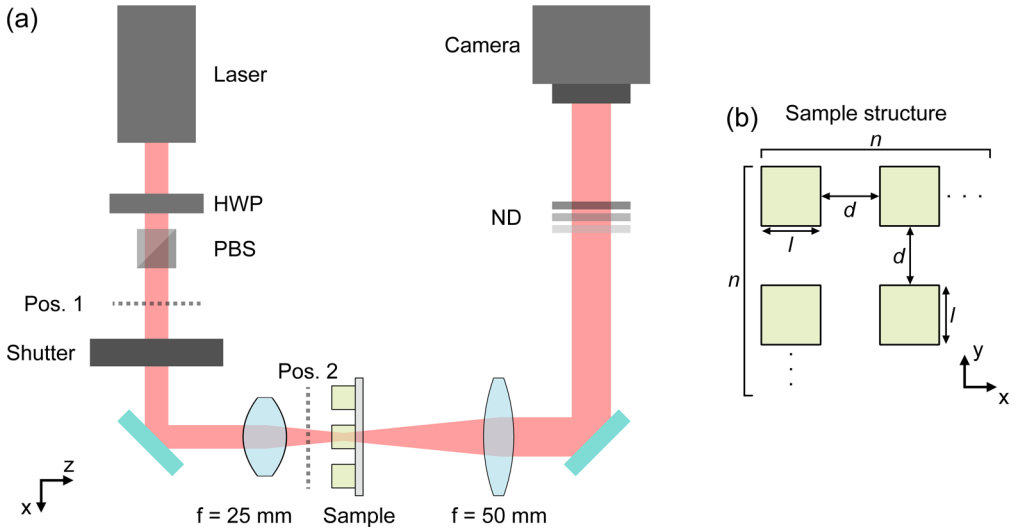

Fig. 1. The setup (a) for inducing damage onto 3D-printed cubes of the photoresist Nanoscribe IP-S. The linearly polarized laser beam is generated by a Stuttgart Instruments Primus laser at 1040 nm and then frequency converted by a Stuttgart Instruments Alpha optical parametric oscillator (OPO), giving wavelengths from 1350 nm to 2050 nm. The beam is then attenuated by a combination of a half wave plate (HWP) and a polarizing beam splitter (PBS). For time-resolved measurements with the accuracy in the millisecond regime, an electronically controlled shutter is used. The beam is focused onto a sample cube, collimated again to twice the size, and hits the beam profile camera sensor after being attenuated by ND-filters to protect the camera from overexposure. The samples (b) consist of equally spaced cube arrays with $l = d = 100$ µm and $n = 10$. The height of each cube in a sample is given by l.

The samples consist of 3D-printed cube arrays of IP-S photopolymer printed onto a glass substrate.

They are printed using the Photonic Professional GT (Nanoscribe GmbH) and have a lateral width of 100 µm with a 100 µm distance in arrays of 10 × 10 cubes. Figure 1(b) schematically indicates the sample geometry. After printing, all cube samples are additionally heat-treated

Optical Materials EXPRESS

at 100 °C, while being UV-exposed for 1 h. This procedure ensures that the cubes are fully polymerized and no local refractive index deviations are present [25].

For damage testing, the samples are placed at the focus position behind a $f = 25$ mm C-coated achromatic lens. After passing the sample, the beam is recollimated by a $f = 50$ mm lens and imaged onto a InGaAs beam-profile camera (VDS Vosskuehler GmbH) protected from an overexposure by a set of ND-filters. With the camera we can image the NIR laser beam profile and perform quantitative evaluations of the variations due to damage.

For determining the average intensity present in the sample, we use the knife-edge test to measure the beam radius and standard Gaussian optics to calculate the secondary beam waist behind the focusing lens, which amounts to 10 µm and 13 µm depending on the wavelength in use. To determine the incident power behind the $f = 25$ mm lens, it is measured at two power-meter positions as shown in the Figure 1. This gives us the ratio to subsequently convert the power measured during the experiment at power-meter position 1 to the power present at the sample.

For damage-detection, we utilize two different methods. The first one is a visual damage-detection approach with a bright-field microscope or differential interference contrast (DIC) microscope, while the second one is an in-situ damage-detection based on the observed mode change of the damaging laser beam after passing the sample by comparing pre and after high-power exposure images.

3. Results and discussion

3.1. Pre-test

To obtain a first impression of the range of damage we are able to induce with our setup, we select a number of wavelengths of interest based on the optimal operation regime of the SI Alpha OPO and considering the desired high-power laser radiation to induce the damage on the samples. Based on this, we choose the wavelengths of 1550 nm, 1700 nm, 1800 nm, and 2000 nm. We conduct a first damage test at the power of ca. 420 mW for the selected wavelengths, as this power is the maximum one for 2000 nm. The results are shown in Figure 2 together with the extinction coefficient for IP-S, which had been previously measured in [25].

This test shows the capability of our setup of damaging IP-S samples at wavelengths indicated in Figure 2(a).

As we expect from the extinction coefficient of the IP-S photopolymer, inducing damage at 1550 nm requires the highest intensity among all wavelengths tested. In our test, we could not induce visually visible damage at this wavelength during a 2 min exposure, even though the average intensity is the highest among four pre-tests. Moving the wavelength further into the IR, the spot size of the focused beam increases, hence the intensities for 1700 nm, 1800 nm, and 2000 nm decrease. At 1700 nm, the extinction coefficient exhibits a peak which causes visible damage to occur even at a lower intensity than at 1550 nm. As we expect for the highest two wavelengths, where the extinction coefficient is larger than at 1550 nm but smaller than at 1700 nm, visible damage occurs with a severity lying somewhere in between. Overall the extinction curve and the severity of the visible damage correlate quite well, which raises the question if intensity is the right quantity to observe, as the power remains constant in this experiment. Would this have been measured at a constant intensity instead, the correlation between damage severity and extinction curve would likely be decreased.

Note that we repeated the experiment three times for each wavelength, i.e., we exposed three different cubes with the same parameters to ensure no variation due to occasional defects. The full version of Figure 2(a) can be found in the Supplement 1 (Figure S1).

Optical Materials EXPRESS

(a)

wavelength	1550 nm	1700 nm	1800 nm	2000 nm
power	436 mW	415 mW	420 mW	419 mW
average intensity	219 kW/cm^2	161 kW/cm^2	171 kW/cm^2	91 kW/cm^2
exposure time	2 min	2 min	2 min	2 min
pre-exposure image	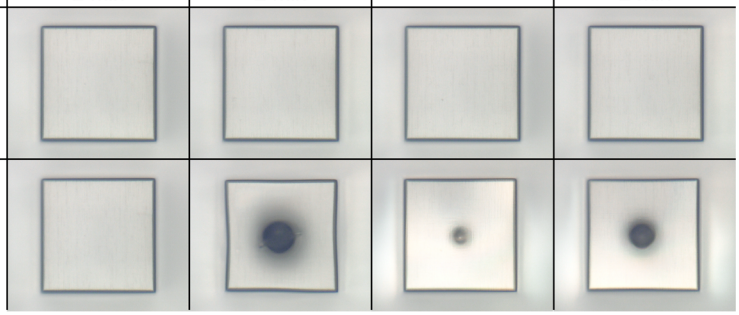			
post-exposure image				

(b)

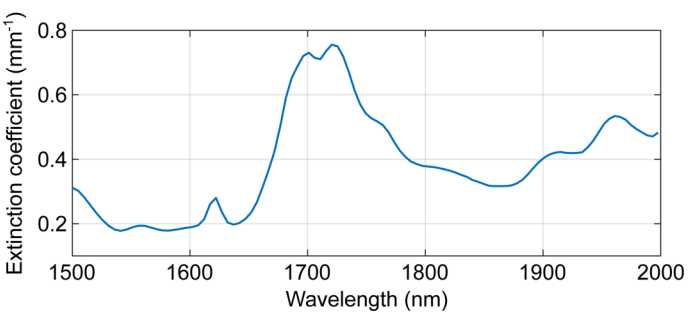

Fig. 2. (a) The images before and after pre-tests conducted on (100 µm)^3 cubes with similar power at each wavelength. For each test, the wavelength, power, average intensity, and exposure times are given. The intensity decrease for higher wavelengths is due to an increasing focus spot size. Most noticeably, damage only occurs for the three highest wavelengths investigated. This is due to the higher absorption of IP-S at over 1650 nm, which can be seen in (b). There also seems to be a correlation between damage severity and extinction. All images were taken with bright-field illumination.

3.2. *Visual inspection of femtosecond laser pulse induced damage*

In the following, we expose a number of cubes on the 10×10 sample with varying intensity and exposure time. In wavelength choice we are limited by the sensitivity of the beam profile camera and the wavelengths capable of inducing damage in our setup, therefore, we choose 1700 nm for better illustration purposes. The damaged cubes are then viewed under an optical microscope (Keyence VHX-6000) to determine which combination of exposure time and intensity and thus dose and fluence damaged the cubes.

Regarding the visual inspection, an important question is what counts as damage. We only consider thermal damage for our evaluation and ignore the defect-driven damage that in our case can be recognized by the the small size of damage compared to the thermal damage which is roughly the size of the laser beam. Hence, any visible deviation from the pre-exposure image, which is highly likely to be caused by thermal effects of the laser radiation on the cube, is counted as damage.

Figure 3 shows the results of damage testing, which are obtained by visual inspection of the sample both under a conventional bright-field optical microscope and under a DIC microscope (Figure 3(a)) for three selected exposure times and intensity values. In Figure 3(a) we can differentiate between the cases, where both the bright-field and the DIC microscope did not show

Optical Materials EXPRESS

any signs of damage (top two images), where both images show significant damage (bottom two images) and where only the DIC image shows signs of damage (two images in the center). From this comparison one can clearly notice the higher sensitivity the DIC microscope inspection achieves. This sensitivity difference then manifests in Figure 3(b, c), which displays the evaluated data points from the corresponding microscope images.

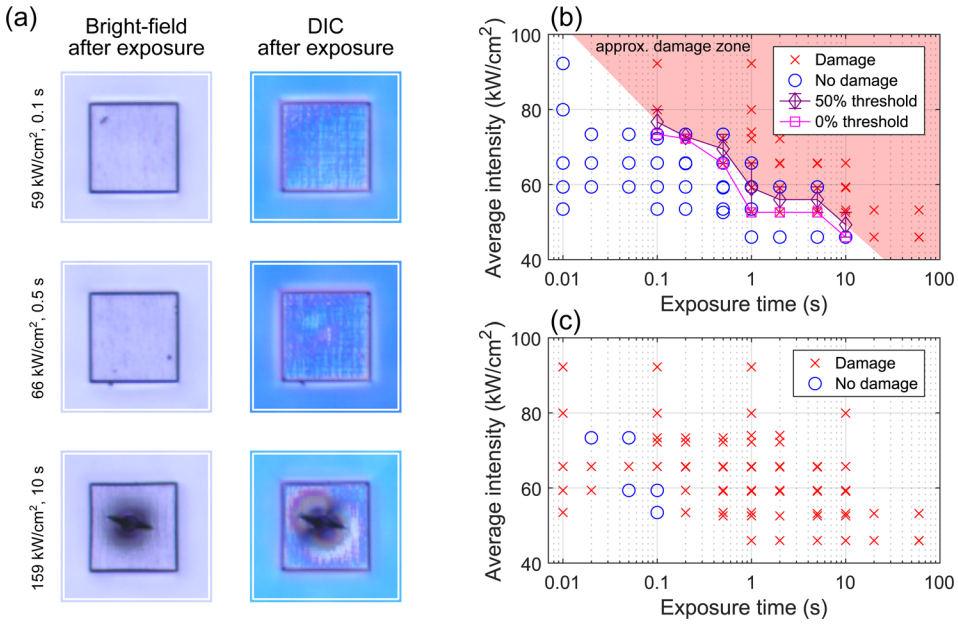

Fig. 3. (a) Images of the laser-exposed cubes obtained with bright-field reflective microscopy and with DIC microscopy. Each bright-field/DIC pair represents the same cube imaged in two different ways. The higher sensitivity of the DIC microscopy can be seen by comparing the appearance of the cube exposed to 66 kW cm^{-2} for 0.5 s (middle row) in the bright-field illuminated image to the DIC image. The cube looks undamaged in the bright-field image but appears clearly damaged in the DIC image. For the other two examples, both inspection methods yield the same result. In (b) and (c) the damage evaluations of the normal and DIC image of all tested cubes are plotted respectively. For the bright-field illumination, 0 % and 50 % threshold estimates are additionally shown. The DIC evaluation is much more sensitive regarding the damage threshold. Consequently, nearly all cubes are counted as damaged.

In Figure 3(b), we display the data points corresponding to the damaged and undamaged cubes extracted from the bright-field microscope image. As expected, a separation of the area of damaged cubes from the undamaged ones can be observed on the 2D plane. In the top right of the plot (approx. damage zone), every cube seems to have experienced damage, and to the bottom left, every cube is undamaged. The crucial part is the transition region where damaged and undamaged results overlap. This overlap could be present due to not perfectly matching the alignment of the sample in both experiments, although it seems relatively consistent and gives, therefore, a statistical view of the damage. For further inspection of the data, we estimate a 50 % and a 0 % damage threshold for multiple exposures. We can do this for any exposure value where there is at least one intensity with a damaged cube and one with an undamaged cube. For the 50 %-threshold, we take the lowest intensity with damage and the highest intensity without damage for every exposure time and calculate the mean value in between. The error bars for this evaluation extend to both points from which we calculate the mean value. For the 0 %-threshold, we take the lowest point of damage for each exposure time. We use the

Optical Materials EXPRESS

same evaluation procedure for the data obtained from the DIC-microscope image (Figure 3(c)), although we omit the threshold lines due to the lack of non-damaged cubes in the DIC image.

In addition to the tests performed at 1700 nm, we also conduct similar measurements at 1550 nm with the same type of samples - cubes with edges of 100 µm length. This time we utilize the full power available at this wavelength from the laser (0.8 W). The exposure times are longer than for the 1700 nm damage tests, since the absorption of the IP-S photopolymer is much lower at 1550 nm than at 1700 nm. Hence, we expect higher damage thresholds at this wavelength.

From a pre-test, we find out that our setup is not able to induce visible damage at an exposure time of 2 min. For the sake of comparison, we take a series of measurements with higher exposure times - 5 min, 15 min, 30 min, 45 min and 60 min - and expose our sample cubes with the 1550 nm laser radiation. Figure 4 depicts the DIC images of these cubes before and after longer exposures together with a bright-field image after the exposures showing the surface of the cubes.

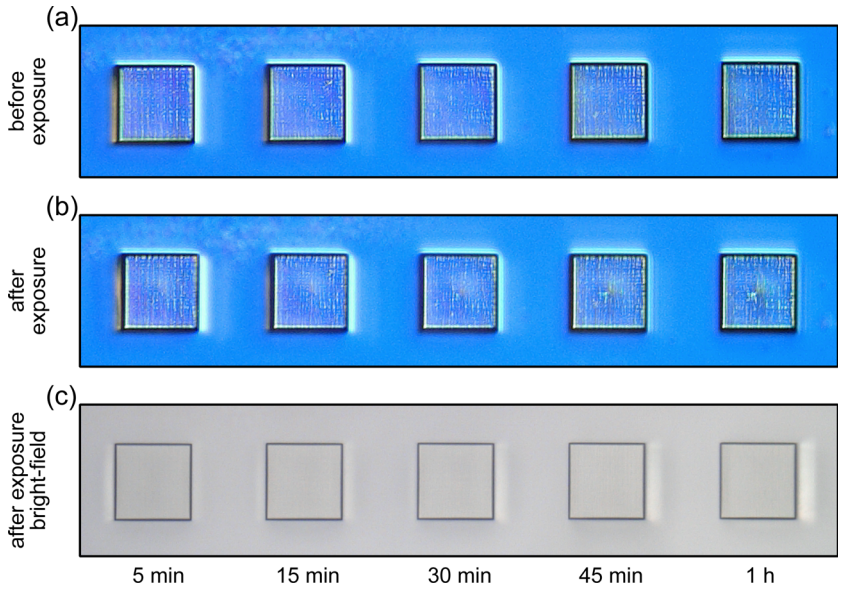

Fig. 4. Images of 100 µm sized cubes pre- and after-exposure to 1550 nm laser radiation. A pre-exposure DIC-image of five 100 µm sized cubes, printed in a row. (b) An after-exposure DIC image with exposure times of 5 min, 15 min, 30 min, 45 min and 60 min, increasing from left to right. The comparison between (a) and (b) displays the visible changes due to this exposure. The bright-field image after the exposure (c) proves that the damage is not occuring on the surface but instead is present only in the bulk of the sample.

As one can see in Figure 4 (b), a slight damage is already visible in the DIC image for the 5 min exposure. Increasing the exposure times up to 1 h, we observe a more noticeable differences between the DIC images of the cube before and after irradiation, indicating more severe damage. In contrast to our previous test, where we saw clear signs of surface damage with a bright-field microscope (burned resist), in this case, damage seems to be only present in the bulk of the sample, as the surface image shows no kind of deformation or melting of the photoresist. Therefore, we believe that the visible changes are only slight differences in the refractive index of the IP-S being amplified by observing it with a DIC microscope. These changes are likely induced by local heating for a longer period of time and are noticeably larger for increased exposure.

The comparison between visual damage detection via bright-field and DIC microscopy shows that the latter method provides greater sensitivity to even slight damage in the bulk of the sample.

Optical Materials EXPRESS

However, this barely noticeable damage might not have a significant influence on the optical performance of a 3D-printed micro-lens for real-world applications.

3.3. Femtosecond laser pulse induced damage inspected via mode change

Since one of the main use cases of the 3D-printed components is optics, i.e., manipulating incident beams in one way or another, we also determine damage based on the in-situ observations of the beam-profile changes behind the samples as we expose them with laser radiation.

For this experiment, we use a beam-profile camera to measure changes of the mode related to damage of the cube. This is carried out by taking two images of the beam profile behind the sample. Except when measuring the thermal lensing effects, the images are always taken at low laser power. This ensures that we only take permanent damage into account and exclude thermal lensing effects. Between taking these two images the cube is exposed to a high intensity of the same laser beam. The two images then are median-filtered, as the beam profile camera shows a significant amount of salt and pepper noise. Afterwards, the images are normalized and subtracted from each other.

Figure 5(a) visualizes the measurement process: on the left-hand side a reference measurement before high-power exposure is shown, while the measured beam-profile after the high-power exposure is shown in the middle. On the right-hand side one can see the difference image between the two measurements. From this difference, a root-mean-square deviation (RMSD) is calculated. This represents the mode change after a high-power exposure.

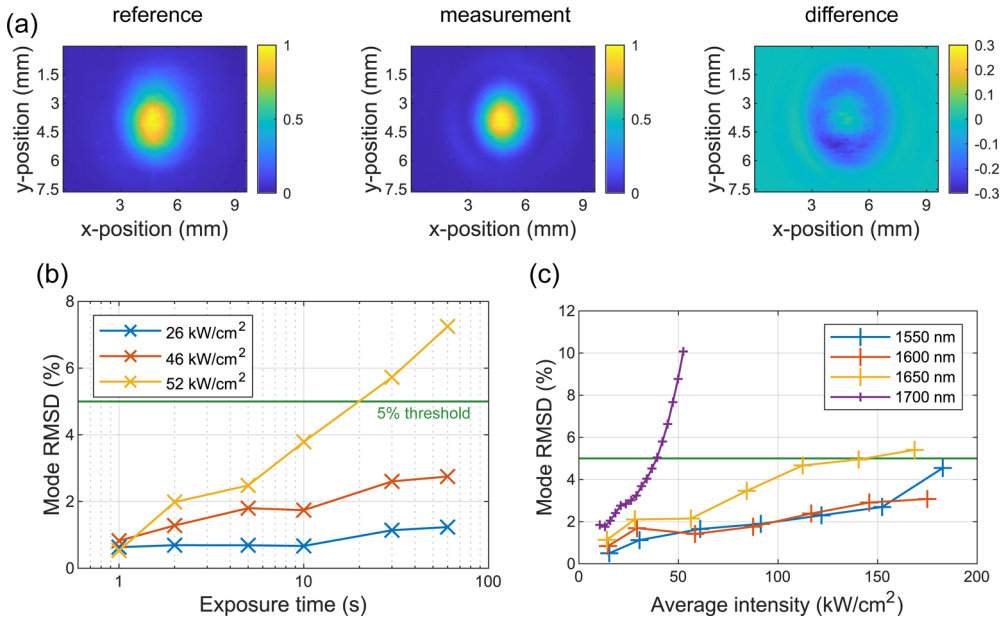

Fig. 5. (a) Left-to-right: A reference image, a measurement image, and the calculated difference image. The two measured images are taken with the beam profile processed afterwards to remove salt and pepper noise of the camera. The measurement image is taken either after a high-power exposure or during a lower power exposure. Graph (b) shows the measured permanent mode changes of the beam profile-images behind the IP-S sample cubes for 1700 nm after exposure with various intensity levels for different exposure times. (c) The measured mode changes between pre-exposure and during exposure at multiple wavelengths for different intensity levels. Quite noticeable is the slightly steeper increase of 1650 nm for higher intensities and the strongly steeper increase at 1700 nm, which is in line with the increased extinction coefficient of IP-S at 1700 nm.

Optical Materials EXPRESS

For the permanent damage evaluation we measure the mode change for multiple intensities and exposure times at a wavelength of 1700 nm. The tested cubes are again $(100\ \mu m)^3$ in size and in a 10×10 grid. The corresponding results are displayed in the Figure 5(b).

For thermal lensing measurements, the second image is taken during a high-power exposure to capture the mode change due to temporal refractive index change in the sample. When measuring the thermal lensing behavior of IP-S, we measure the mode change for multiple intensities and wavelengths. The latter are chosen in a range where an increase of damage is suspected. For each wavelength a separate cube is measured. After ramping up the power on the cube with the highest expected damage (at $\lambda = 1700$ nm), we take a low-power image to confirm that all damage observed in the data is of temporary nature, which is what we are after. Figure 5(c) depicts the results of thermal lensing measurements.

The evaluation confirms that when measuring permanent mode change (damage) after different exposure times and intensities, the perceived mode change rises approximately logarithmically with the exposure time. Also, there was no significant damage detected for the lowest intensity of 26 kW cm^{-2}. When observing the mode change during the exposure to detect changes due to thermal lensing, we measure a linear increase of the mode change with the intensities for wavelengths of 1650 nm and below and an exponential increase for 1700 nm. This is in line with the extinction coefficient measured in [25] shown in Figure 2, which shows an increase in extinction between 1650 nm and 1700 nm. This is exactly where we see an increased effect of thermal lensing, which is expected, as thermal lensing is induced by a thermal gradient that becomes steeper for higher absorption.

3.4. Nanosecond laser pulse damage visually inspected according to ISO 21254

With a different setup at the Institute for Technical Physics at the German Aerospace Center (DLR), which can perform measurements in conformity with the ISO 21254, we also measure the damage threshold of IP-S for nanosecond pulses at 1064 nm. For this, we prepare a sample of a thin IP-S layer by placing two glass substrates on top of each other with an IP-S droplet in between. Afterwards, we harden the IP-S with a UV-lamp. After the UV-exposure, the top glass substrate is peeled off to obtain a smooth IP-S surface. The thickness of the sample prepared in such a way is ca. 0.1 mm, which is well suitable for our further testing and directly comparable to the sizes of 3D-printed cubes from previous tests. Despite a few µm-sized bubbles and inclusions, the sample is quite homogeneous across the entire area of 20×20 mm^2 (see Supplement 1, Figure S2).

We conduct the following experiments: s-on-1 with 100 pulses (Figure 6(a)), and s-on-1 with 10 000 pulses (Figure 6(b)). The exposed sites are chosen 1 mm apart. The $1/e^2$ diameter of the beam used for testing is 342 µm. The pulse repetition rate was 100 Hz and the pulse duration was 10 ns (full width at half maximum). After exposures, the damage is observed using a DIC microscope.

As we expect, the results of experiments performed with ns-pulses differ significantly from the results of fs-pulsed testing: With the damage threshold of 1.5 –1.7 J cm^{-2} for the nanosecond pulses at 1064 nm (Figure 6) the results differ with more than factor 1000 from a threshold of 1.15 mJ cm^{-2} for our measurement at femtosecond pulses with 1700 nm. This discrepancy arises from the fact that we are likely observing different damage types in both experiments. With such a high repetition rate and quite low pulse energy, as we use in the femtosecond experiments, the radiation is much more similar to a cw-regime. This radiation then gradually heats up the material and does not induce as much heat at a time at defect sites, which are responsible for generating defect-driven damage. On the other hand, using nanosecond-pulsed radiation with much higher fluence, we observe predominantly the defect-driven damage at a lower intensity than the one required to induce thermal damage. Therefore, one should not directly compare the two vastly different fluence values.

Optical Materials EXPRESS

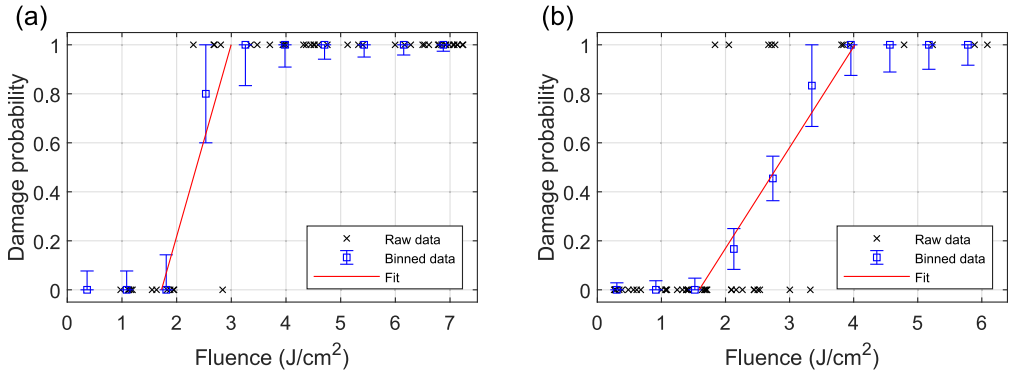

Fig. 6. The damage threshold extrapolation of the data for the 100-on-1 (a) and 10000-on-1 (b) damage test measured with an ISO 21254 conform setup. The raw damage data is binned and then fitted using a cumulative approach with weighted data points.

3.5. Application examples

As was already mentioned, one of the main use-cases of such 3D-printing photoresists like IP-S is manufacturing micro-optics. So far, there were only a few mentions of applying laser radiation above 1W power to the 3D-printed micro-lenses [16]. Meanwhile, one of the trends in the laser industry is to miniaturize laser systems, while maintaining high output power for such applications as optical trapping, sensing, and imaging. Optical fibers and fiber-coupled lasers are quite suitable platforms for such compact systems. Hence, we choose some widely used wavelengths out of the available for us - 915 nm in the cw-regime, produced by a fiber-coupled diode laser with the maximum output power slightly above 10 W, and 1040 nm of the SI Primus fs-laser with the maximum output power of 8 W. Both of these wavelengths are widely used for pumping solid-state systems for diverse applications. For the fs-tests we coupled the light into the 1060XP (Thorlabs GmbH) single-mode fiber, to make the comparison between the cw- and fs-performance easier.

Looking at the extinction curve from [25], we can see that the extinction at 915 nm and 1040 nm is significantly lower than at 1700 nm (ca. 10 times lower), which we have extensively studied already. Hence, we expect higher maximum output power, which can be used with the 3D-printed micro-optics without destroying them.

Using the knowledge gained during the LIDT-testing of IP-S polymer, we produce some optics tailored for high-power laser systems. At first, we print a singlet aspheric lens on a fiber-coupled 915 nm pump diode. For that, we cleave the multimode pump-fiber with a diameter of 125 µm and splice a 565 µm long no-core fiber piece with a diameter of 250 µm onto it using a Vytran GPX 3800 automated glass processor. The larger no-core fiber piece allows for efficient beam expansion in order to use the full lens aperture of 250 µm diameter. After printing, the 65 µm thick lens sits perfectly centered on the no-core fiber piece.

Figure 7 depicts the setup we use to perform beam-profile measurements and the output power measurements. The pump-diode with the 3D-printed lens is mounted in an Elliot-Martock fiber holder on a 3D-stage. The beam exiting the fiber is collimated by a 50 mm lens and passes through a series of ND-filters, which protect the camera from the overexposure and damage. Then, the second 50 mm lens focuses the beam onto a camera sensor (or a power-meter for power measurements). Thus, we utilize 1:1 imaging of the focus produced by the fiber optics.

During the experiment, we increase the current of the pump-diode and observe changes in the mode behind the fiber lens. We verify the power deduced from the diode characteristic by

Optical Materials EXPRESS

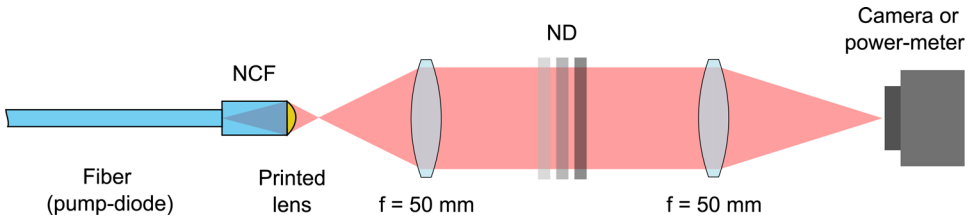

Fig. 7. A scheme of the experimental setup for damage threshold testing of the micro-optics 3D-printed onto a 915 nm fiber-coupled pump-diode. The fiber with a spliced no-core fiber piece and 3D-printed lens is mounted in a fiber holder. The light from the fiber is focused at the distance of ca. 300 µm. The focal spot is then projected without magnification by two 50 mm lenses onto a camera sensor for mode profiling. A set of ND-filters in the parallel beam protects the camera from the high-intensity laser radiation. The camera is then substituted by a power-meter and ND-filters are taken out to measure the full incident power, corresponding to the mode-picture.

replacing the camera with the power meter and removing the ND filters to ensure the correct measurement.

Figure 8 displays the microscope images of the pump-fiber with the 3D-printed lens before and after the 10.5 W exposure, as well as the mode pictures at the low and high laser power and their difference. During the experiment, the lens was exposed to 10.5 W power for roughly 2 min. This power corresponds to an average intensity of 22 kW cm^{-2}.

In Figure 8(a, b) one can see two laser modes taken by the laser power of 1.75 W as the reference and 10.5 W as the high-power operation. The two modes are comparable in shape, but most importantly, there is no significant damage in the regions with extremely high intensity. Figure 8(c) depicts the difference of the two modes. The corresponding RMSD is 7%, which is slightly higher than the threshold values set previously. However, for this application one could use a higher threshold for the mode change, as in the first place one would care about the pump power delivery to a particular area. Furthermore, the initial quality of the mode at the low power is not the best by itself, which has to do with the pump-diode quality. Finally, in the angled image with focus-stacking in Figure 8(f), one can see that the lens remains intact even though some mechanical damage is visible on the fiber itself.

We conduct an experiment with a similar setup, but this time using a single-mode 1060XP fiber (Thorlabs GmbH) with a 3D-printed 65 µm thick lens on it. Due to the smaller core size and smaller NA of the fiber compared to the multimode pump-fiber, we splice a longer no-core fiber piece of 1160 µm onto the single-mode fiber to use the entire 250 µm aperture of the lens. We couple 1040 nm fs-pulsed laser light (Stuttgart Instruments GmbH Primus) into the cleaved fiber using a microscope objective and an Elliot-Martock stage. At the output, we image the focal spot using a 5x telescopic system.

We again increase the power of the laser gradually starting from ca.35 mW. Figure 9(a) depicts the corresponding mode profile while measuring 37.5 mW after the fiber lens. We are able to go up to 4.5 W output power (Figure 9(b), hold it for several minutes, and revert to the low power multiple times without any noticeable change in the mode shape. The difference between the two modes is displayed in Figure 9(c). The RMSD value in this case is below 3 %. Hence, we can state that no damage has occurred after the 4.5 W exposure with a fs-laser, which corresponds to an average intensity of 12 kW cm^{-2}. Figure 9 also depicts the microscope images of the tested fiber before (Figure 9(d)) and after (Figure 9(e)) high-power exposure in corresponding angled views under different illuminations.

It is important to note that this value is limited not by the 3D-printed lens itself but rather by the coupling efficiency at the input side of the fiber. In our experiments, we used end caps

Optical Materials EXPRESS

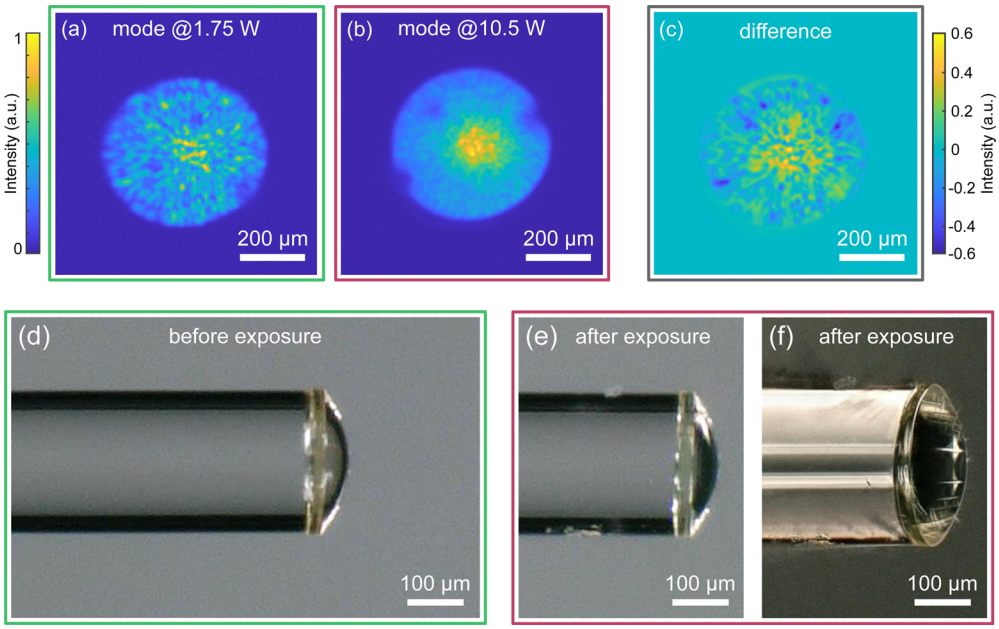

Fig. 8. Evaluation of the optical performance of the cw fiber-coupled pump-diode with 3D-printed micro-optics. Comparing the images of the laser mode at a relatively low output power of 1.75 W (a) and at a higher power of 10.5 W (b), one can see that the beam remains complete and preserves its initial shape quite well. Darker spots in (b) are due to damaged beam-profile camera sensor. Similar spots are visible in (a), although being less prominent probably because of different exposure time settings. In (c) the difference of the two modes is shown. The RMSD value for this case is 7%. Partially, this value has to do with the poor initial beam quality of the pump-diode at low currents, i.e., low output power levels. (d) Microscope image of a fiber with a 3D-printed lens before the high-power fs-pulsed laser exposure. (e) Microscope image of a fiber with a 3D-printed lens after the high-power fs-pulsed laser exposure. The slightly darker appearance of the lens after exposure in the overview image is mostly due to different positioning of the fiber under the microscope. (f) An angled close-up view of the same fiber lens after the high-power fs-pulsed laser exposure. In (e) and (f) it is clearly visibly that the surface of the lens remains intact.

of 410 µm length and 125 µm diameter at the in-coupling side. With this, we achieved output powers above 5 W without observing any damage on the lens, but the input side got damaged by a visible explosion rather quickly.

Comparing our experiments and findings with cw- and fs-radiation, we assume that the damage mechanisms in both cases should be rather similar and predominantly of a thermal nature. The difference in the achieved values of average intensities arises due to a number of factors. Firstly, the power distribution within a mode might play a role: one could expect that a top-hat-like beam shape would cause less damage than a Gaussian-shaped beam with comparable intensity. Secondly, as was already mentioned, in our fs-pulsed experiments we were limited through the in-coupling side of the fiber. One could splice an end-cap of a bigger diameter to the lensed fiber in order to be able to use higher power levels, but with our setup, we were also limited with the input laser power of ca. 8 W. Extrapolating the results from the previous sections, we would expect a 5% RMSD threshold around 50 kW cm^{-2}.

In both cases, considering the lower extinction values in comparison to 1700 nm, the 3D-printed fiber lenses are likely operating under the severe damage threshold and could be used with the mentioned powers for a prolonged time. However, this would still require a thorough

Optical Materials EXPRESS

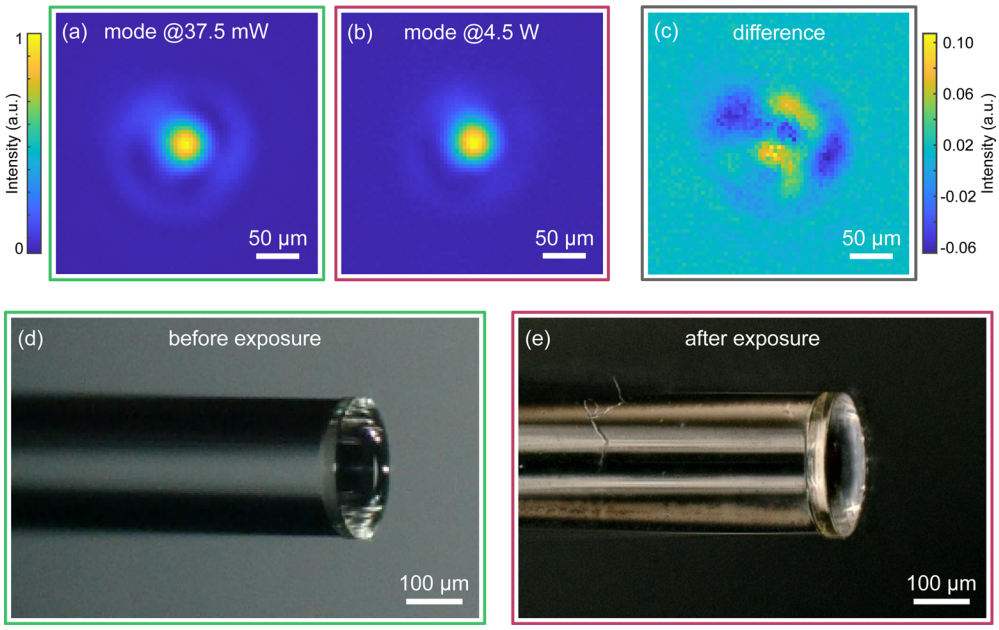

Fig. 9. Evaluation of the optical performance of the single-mode fibers with 3D-printed micro-optics. (a) and (b) display the laser mode imaged with the beam-profile camera at low and high-power fs-pulsed laser exposure, respectively. One can see that the beam remains Gaussian and shows no significant mode deviations. This is even more obvious in (c), where the difference of the two modes is depicted. The corresponding RMSD is 3%. (d) Microscope image of a fiber with a 3D-printed lens before the high-power fs-pulsed laser exposure. (e) Microscope image of a fiber with a 3D-printed lens after the lens after the high-power fs-pulsed laser exposure. The close-up images of the lens are both taken under an angle to emphasize the clear optical top surface in both cases. Differences in the appearance of the images are mainly due to fiber positioning under the tilted microscope imaging system. In (e) it is clearly visibly that the surface of the lens remains intact compared to its initial state.

verification through long-term measurements, e.g., overnight output power stability, together with the observation of the output modes.

4. Conclusion

In conclusion, we conducted a first systematic study on the laser-induced damage thresholds of IP-S photopolymer, which is widely used in 3D-printing of micro-optics. Using a femtosecond laser with the repetition rate of 40 MHz we exposed several samples with arrays of 3D-printed cubes. We used three different damage-observation methods: conventional optical bright-field microscopy, DIC-microscopy, and in-situ mode change. The first method provides higher threshold values compared to the more sensitive DIC-microscopy, but we could not confirm the significance of such damage (visible only under a DIC-microscope) on the mode shape. Arguably, the latter is more important for the real-world usage of 3D-printed micro-optics, hence, one could rely solely on mode change method for further studies of such small optics.

The experiments with femtosecond-pulsed radiation and the evaluation based on mode change yielded a damage threshold of 46 kW cm^{-2} at 1700 nm which corresponds to a fluence of 1.15 mJ cm^{-2} for a pulse duration of 550 fs. We also separated the thermal lensing effects from

Optical Materials EXPRESS

permanent thermal damage in this regime. Moreover, we found some correlation between measured earlier extinction coefficient [25] and the damage threshold for fs-pulsed laser radiation for IP-S. Although this correlation appears to be strong for wavelengths in the range between 1550 −1700 nm and less obvious for the higher wavelength, additional experiments and studies should be done to postulate the relationship between extinction coefficient and damage threshold precisely, as it could allow generalized predictions of the threshold power for a known wavelength to be used with a particular 3D-printed micro-lens. This knowledge then could be extrapolated to the already measured properties of other photopolymers such as IP-Dip, IP-Visio, OrmoComp etc., further broadening the usability of 3D-printed optics in high-power applications.

We also performed ISO21254-conform measurements at 1064 nm with nanosecond laser, namely s-on-1 with 100 pulses and s-on-1 with 10 000 pulses. These tests resulted in a damage threshold of 1.5 −1.7 J cm^{-2}. The difference between these values and the damage threshold we found for fs-pulsed radiation can be explained by a different nature of the damage observed after the exposure: for the femtosecond radiation the damage is more of the thermal nature, while with the high energy nanosecond pulses we were able to observe defect-driven damage, which usually occurs earlier than thermal one.

Finally, we presented some examples of the 3D-printed high-power optics: a 915 nm cw-fiber pump-diode with a 3D-printed lens, reaching 10.5 W output power or 22 kW cm^{-2} and preserving the mode shape it had at low power and also a single-mode fiber at 1040 nm, reaching 4.5 W or 12 kW cm^{-2} output power with fs-pulsed radiation. These results show that such small 3D-printed optics can be used for prolonged time in fiber-based application, where high laser power is crucial, such as sensing, laser processing of materials and optical trapping.

Despite our findings, the complete LIDT-testing of IP-S and other common photopolymers for 3D printing remains highly important. Also, to confirm that the damage is not accumulating with time, one would need to conduct a series of measurements over several hours with steady high-power exposure, as this remained outside the scope of this work due to technical limitations of the measurement setups.

Funding. European Research Council (PoC 3DPRINTEDOPTICS); Bundesministerium für Bildung und Forschung (PRINTOPTICS, Q.Link.X, QR.X); Deutsche Forschungsgemeinschaft (GRK 2642); Gips-Schüle-Stiftung; Carl-Zeiss-Stiftung (EndoPrint3D).

Acknowledgments. The authors thank Simon Angstenberger for assistance with the fs-pulsed setup as well as Mario Hentschel and Moritz Floess for fruitful discussions.

Disclosures. The authors declare no conflicts of interest.

Data Availability. Data underlying the results presented in this paper are not publicly available at this time but may be obtained from the authors upon reasonable request.

Supplemental document. See Supplement 1 for supporting content.

References

1. M. Deubel, G. von Freymann, M. Wegener, S. Pereira, K. Busch, and C. M. Soukoulis, "Direct laser writing of three-dimensional photonic-crystal templates for telecommunications," Nat. Mater. **3**(7), 444–447 (2004).
2. M. Malinauskas, A. Žukauskas, S. Hasegawa, Y. Hayasaki, V. Mizeikis, R. Buividas, and S. Juodkazis, "Ultrafast laser processing of materials: from science to industry," Light: Sci. Appl. **5**(8), e16133 (2016).
3. T. Gissibl, S. Thiele, A. Herkommer, and H. Giessen, "Two-photon direct laser writing of ultracompact multi-lens objectives," Nat. Photonics **10**(8), 554–560 (2016).
4. M. Schmid, F. Sterl, S. Thiele, A. Herkommer, and H. Giessen, "3D printed hybrid refractive/diffractive achromat and apochromat for the visible wavelength range," Opt. Lett. **46**(10), 2485–2488 (2021).
5. S. Ristok, S. Thiele, A. Toulouse, A. M. Herkommer, and H. Giessen, "Stitching-free 3D printing of millimeter-sized highly transparent spherical and aspherical optical components," Opt. Mater. Express **10**(10), 2370–2378 (2020).
6. A. Toulouse, J. Drozella, P. Motzfeld, N. Fahrbach, V. Aslani, S. Thiele, H. Giessen, and A. M. Herkommer, "Ultra-compact 3D-printed wide-angle cameras realized by multi-aperture freeform optical design," Opt. Express **30**(2), 707–720 (2022).
7. I. V. A. K. Reddy, A. Bertoncini, and C. Liberale, "3D-printed fiber-based zeroth- and high-order Bessel beam generator," Optica **9**(6), 645–651 (2022).

Optical Materials EXPRESS

8. M. Schmid and H. Giessen, "Stress-induced birefringence in 3D direct laser written micro-optics," Opt. Lett. **47**(22), 5789–5792 (2022).
9. L. Siegle, S. Ristok, and H. Giessen, "Complex aspherical singlet and doublet microoptics by grayscale 3D printing," Opt. Express **31**(3), 4179–4189 (2023).
10. J. Li, S. Thiele, B. C. Quirk, R. W. Kirk, J. W. Verjans, E. Akers, C. A. Bursill, S. J. Nicholls, A. M. Herkommer, H. Giessen, and R. A. McLaughlin, "Ultrathin monolithic 3D printed optical coherence tomography endoscopy for preclinical and clinical use," Light: Sci. Appl. **9**(1), 124 (2020).
11. A. Asadollahbaik, S. Thiele, K. Weber, A. Kumar, J. Drozella, F. Sterl, A. M. Herkommer, H. Giessen, and J. Fick, "Highly Efficient Dual-Fiber Optical Trapping with 3D Printed Diffractive Fresnel Lenses," ACS Photonics **7**(1), 88–97 (2020).
12. P. Ruchka, S. Hammer, M. Rockenhäuser, R. Albrecht, J. Drozella, S. Thiele, H. Giessen, and T. Langen, "Microscopic 3D printed optical tweezers for atomic quantum technology," Quantum Sci. Technol. **7**(4), 045011 (2022).
13. A. Asadollahbaik, A. Kumar, M. Heymann, H. Giessen, and J. Fick, "Fresnel lens optical fiber tweezers to evaluate the vitality of single algae cells," Opt. Lett. **47**(1), 170–173 (2022).
14. M. Schmid, S. Thiele, A. Herkommer, and H. Giessen, "Adjustment-free two-sided 3D direct laser writing for aligned micro-optics on both substrate sides," Opt. Lett. **48**(1), 131–134 (2023).
15. C. R. Ocier, C. A. Richards, D. A. Bacon-Brown, *et al.*, "Direct laser writing of volumetric gradient index lenses and waveguides," Light: Sci. Appl. **9**(1), 196 (2020).
16. P.-I. Dietrich, M. Blaicher, I. Reuter, M. Billah, T. Hoose, A. Hofmann, C. Caer, R. Dangel, B. Offrein, U. Troppenz, M. Moehrle, W. Freude, and C. Koos, "In situ 3D nanoprinting of free-form coupling elements for hybrid photonic integration," Nat. Photonics **12**(4), 241–247 (2018).
17. H. Ren, J. Jang, C. Li, A. Aigner, M. Plidschun, J. Kim, J. Rho, M. A. Schmidt, and S. A. Maier, "An achromatic metafiber for focusing and imaging across the entire telecommunication range," Nat. Commun. **13**(1), 4183 (2022).
18. S. Chu, J. E. Bjorkholm, A. Ashkin, and A. Cable, "Experimental Observation of Optically Trapped Atoms," Phys. Rev. Lett. **57**(3), 314–317 (1986).
19. D. Frese, B. Ueberholz, S. Kuhr, W. Alt, D. Schrader, V. Gomer, and D. Meschede, "Single Atoms in an Optical Dipole Trap: Towards a Deterministic Source of Cold Atoms," Phys. Rev. Lett. **85**(18), 3777–3780 (2000).
20. M. Sartison, K. Weber, S. Thiele, L. Bremer, S. Fischbach, T. Herzog, S. Kolatschek, M. Jetter, S. Reitzenstein, A. Herkommer, P. Michler, S. Luca Portalupi, and H. Giessen, "3D printed micro-optics for quantum technology: Optimised coupling of single quantum dot emission into a single-mode fibre," Light: Adv. Manuf. **2**(2), 103 (2021).
21. A. Butkutė, L. Čekanavičius, G. Rimšelis, D. Gailevičius, V. Mizeikis, A. Melninkaitis, T. Baldacchini, L. Jonušauskas, and M. Malinauskas, "Optical damage thresholds of microstructures made by laser three-dimensional nanolithography," Opt. Lett. **45**(1), 13–16 (2020).
22. A. Žukauskas, G. Batavičiūtė, M. Ščiuka, T. Jukna, A. Melninkaitis, and M. Malinauskas, "Characterization of photopolymers used in laser 3D micro/nanolithography by means of laser-induced damage threshold (LIDT)," Opt. Mater. Express **4**(8), 1601–1616 (2014).
23. D. Gailevicius, R. Zvirblis, K. Galvanauskas, G. Bataviciute, and M. Malinauskas, "Calcination-Enhanced Laser-Induced Damage Threshold of 3D Micro-Optics Made with Laser Multi-Photon Lithography," Photonics **10**(5), 597 (2023).
24. "ISO 21254-2:2011; Lasers and Laser-Related Equipment–Test Methods for Laser-Induced Damage Threshold," Standard, International Organization for Standardization, Geneva, CH (2011).
25. M. Schmid, D. Ludescher, and H. Giessen, "Optical properties of photoresists for femtosecond 3D printing: refractive index, extinction, luminescence-dose dependence, aging, heat treatment and comparison between 1-photon and 2-photon exposure," Opt. Mater. Express **9**(12), 4564–4577 (2019).